Maximum Aperture Power Transmission in Lossy Homogeneous Matters

Maximum Aperture Power Transmission in Lossy Homogeneous Matters

A. Razavi, R. Maaskant, *Senior Member, IEEE,* J. Yang, *Senior Member, IEEE,* and M. Viberg, *Fellow, IEEE*

***Abstract*—We apply array signal processing techniques to the transmitting aperture field modes in order to determine the optimal field distribution that maximizes the power transmission through lossy media between a transmitting and an ideally receiving antenna aperture. The optimal aperture distribution is then used as a reference field for developing curves applicable to the design of many near-field systems, such as for the detection of foreign objects in lossy matters (e.g. food contamination detectors), wireless charging of batteries of human body implanted devices, and for in-body communication systems.**

***Index Terms*—Near field focusing, array signal processing.**

I. Introduction

FOCUSING the near-field (NF) radiated power from an antenna has been an important research topic for a long time. For instance, in [1], [2], a spherical phase front of the aperture field is used to focus the energy at a certain distance in the Fresnel zone. Sherman [1] has shown that the electric field on the focal plane near the axis of such a focused aperture field exhibits typical far-field properties, e.g., a tapered aperture field will result in decreased sidelobe levels, an increased beamwidth as well as a reduced gain. Conversely, for an inverse taper, Hansen [2] demonstrated that low axial lobes before and after the focal distance are to be expected, at the cost of sidelobe and gain level degradations in the focal plane. Graham [3] shaped the axial pattern of NF focusing antennas in lossless media through far-field pattern synthesis based methods, in which the focal distance is still set by the aperture phase distribution, and where the control over the axial pattern is traded against the tranverse pattern quality. Focused apertures have been realized by employing large microstrip arrays or Fresnel zone plate lenses [4], [5]. Recently, Sanghoek et al. [6] proposed a two-port network model to optimize the coupling efficiency between an infinite sheet of magnetic current density and a combination of electric and magnetic dipoles embedded in a planar multilayered medium. It was found that the axial pattern, or forelobes and aftlobes, cannot be defined for a monotonously decreasing NF in a lossy medium, therefore the 3dB NF beam radius becomes a useful parameter for the characterization of NF-focusing antennas [7].

We propose to apply array signal processing techniques to the transmitting aperture field modes in order to determine the optimal field distribution that maximizes the power transmission between a transmitting and an ideally receiving antenna aperture in a lossy homogeneous media. This not only provides us with the fundamental insight on how to achieve the best possible focus in a manner that is more generic than an analytical approach [8], but it also allows us to explore the fundamental limits of NF-focusing antennas and constitutes the first step in a design procedure as one can now independently match the aperture fields of our transmitting and receiving antennas to the optimal ones (a concept also used for conjugate-field-matched focal plane array antennas [9]). Optimal design curves will be presented for several representative cases. The herein presented theoretical study excludes the actual design process of specific transmitting and receving antennas for generality.

The authors are with the Signals and Systems Department of the Chalmers University of Technology, Gothenburg, Sweden, e-mail: aidin.razavi@chalmers.se, rob.maaskant@chalmers.se, jian.yang@chalmers.se and viberg@chalmers.se.

This work is financed by a Swedish Research Council grant.

Manuscript received May 20, 2014; revised August 1, 2014.

II. Problem Description

The NF system in Fig. 1 comprises of a transmitting and a receiving (aperture) antenna embedded in a lossy homogeneous medium whose intrinsic impedance is η. It may represent a solid or a flow of liquid matter. The objective is to maximize the power coupling between the transmitting and receiving aperture antennas. In many applications the receiver size is limited, such as in NF power transfer and/or communication systems involving a large antenna outside and an implanted device inside the human body. Although several receiver aperture sizes will be examined, no optimization is done on the receiving antenna as it is assumed to be conjugately impedance and field matched to the receiving aperture fields, thereby harvesting all the power passing through it.

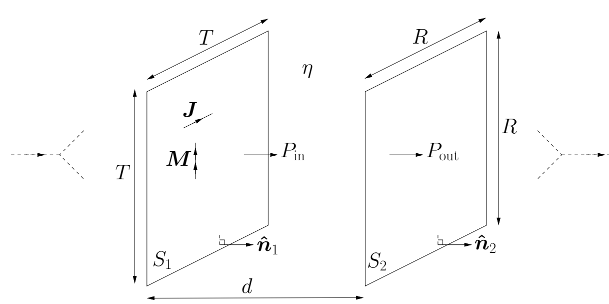

Fig. 1. Power coupling between two apertures separated by a lossy medium.

III. Optimization Procedure Formulation

The goal is to determine the equivalent aperture current distribution that maximizes the NF coupled power between the source and observation apertures S_1 and S_2, respectively, as shown in Fig. 1. Since the fields emanating from the source aperture S_1 are directive in nature, the influence of the ground plane (GP) at the transmit side is neglected. Also, since the medium is very lossy, any backscattered field at the receiving side is assumed to have negligible effect on the transmitting side. Finally, edge diffraction of the GP aperture at the receiving side is neglected. Hence, the NF focusing fields in between S_1 and S_2 can be regarded as being generated by the unknown source currents $\boldsymbol{J}$ and $\boldsymbol{M}$ that radiate in a homogeneous medium. The design problem at hand is finding $\boldsymbol{J}$ and $\boldsymbol{M}$ such that the power transfer between S_1 and S_2 is maximized.

The total received power P_{out} at S_2 is

$$P_{\text{out}} = \frac{1}{2}\mathfrak{Re}\left\{\int_{S_2}[\boldsymbol{E}\times\boldsymbol{H}^*]\cdot\hat{\boldsymbol{n}}_2\,\mathrm{d}S\right\} \tag{1}$$

where the E- and H-fields are generated by $\boldsymbol{J}$ and $\boldsymbol{M}$ as

$$\boldsymbol{E}(\boldsymbol{J},\boldsymbol{M}) = \boldsymbol{E}_J(\boldsymbol{J}) + \boldsymbol{E}_M(\boldsymbol{M}) \tag{2a}$$

$$\boldsymbol{H}(\boldsymbol{J},\boldsymbol{M}) = \boldsymbol{H}_J(\boldsymbol{J}) + \boldsymbol{H}_M(\boldsymbol{M}). \tag{2b}$$

Next, $\boldsymbol{J}$ and $\boldsymbol{M}$ are each expanded in N basis functions as

$$\boldsymbol{J} = \sum_{n=1}^{N} j_n\boldsymbol{f}_n(\boldsymbol{r}), \quad \text{and} \quad \boldsymbol{M} = \sum_{n=1}^{N} m_n\boldsymbol{g}_n(\boldsymbol{r}) \tag{3}$$

where the unknown expansion coefficient vectors $\mathbf{j} = [j_1, j_2, \ldots, j_N]^T$ and $\mathbf{m} = [m_1, m_2, \ldots, m_N]^T$ are yet to be determined. Substituting (3) in (2), and then in (1), and by introducing the complex power between basis functions as $P_{pq}^{AB} = \int_{S_2}[\boldsymbol{E}_A(\boldsymbol{f}_p)\times\boldsymbol{H}_B^*(\boldsymbol{g}_q)]\cdot\hat{\boldsymbol{n}}_2\,\mathrm{d}S$, where $\{A,B\}\in\{J,M\}$, yields for the total output power

$$P_{\text{out}} = \frac{1}{2}\mathfrak{Re}\Bigg\{\sum_{p=1}^{N}\sum_{q=1}^{N} j_pP_{pq}^{JJ}j_q^* + j_pP_{pq}^{JM}m_q^* + \ldots \\ m_pP_{pq}^{MJ}j_q^* + m_pP_{pq}^{MM}m_q^*\Bigg\} \tag{4}$$

or, in matrix-vector form,

$$P_{\text{out}} = \frac{1}{2}\mathfrak{Re}\left\{\begin{bmatrix}\mathbf{j}\\\mathbf{m}\end{bmatrix}^H\begin{bmatrix}\mathbf{P}^{JJ} & \mathbf{P}^{JM}\\\mathbf{P}^{MJ} & \mathbf{P}^{MM}\end{bmatrix}^*\begin{bmatrix}\mathbf{j}\\\mathbf{m}\end{bmatrix}\right\} \tag{5}$$

$$= \frac{1}{2}\mathfrak{Re}\{\mathbf{w}^H\mathbf{P}_{\text{out}}\mathbf{w}\} \tag{6}$$

where we have taken the conjugate of the Poynting vector, and where we have introduced

$$\mathbf{w} = \begin{bmatrix}\mathbf{j}\\\mathbf{m}\end{bmatrix}, \quad \text{and} \quad \mathbf{P}_{\text{out}} = \begin{bmatrix}\mathbf{P}^{JJ} & \mathbf{P}^{JM}\\\mathbf{P}^{MJ} & \mathbf{P}^{MM}\end{bmatrix}^*. \tag{7}$$

The input power P_{in} at the aperture is computed through the aperture equivalent currents, i.e., $\boldsymbol{E}_a = \hat{\boldsymbol{n}}_1\times\boldsymbol{M}$ and $\boldsymbol{H}_a = \boldsymbol{J}\times\hat{\boldsymbol{n}}_1$, so that the Poynting vector integral reduces to

$$P_{\text{in}} = \frac{1}{2}\mathfrak{Re}\left\{\int_{S_1}[\boldsymbol{J}^*\times\boldsymbol{M}]\cdot\hat{\boldsymbol{n}}_1\,\mathrm{d}S\right\} \tag{8}$$

Next, by substituting (3) in (8), P_{in} becomes

$$P_{\text{in}} = \frac{1}{2}\mathfrak{Re}\left\{\mathbf{j}^H\mathbf{A}\mathbf{m}\right\} \tag{9}$$

where A_{pq} are the complex powers radiated by current basis functions, given by

$$A_{pq} = \int_{S_1}\left[\boldsymbol{f}_p^*\times\boldsymbol{g}_q\right]\cdot\hat{\boldsymbol{n}}_1\,\mathrm{d}S. \tag{10}$$

By padding $\mathbf{A}$ with zeros and forming $\mathbf{P}_{\text{in}}$ as

$$\mathbf{P}_{\text{in}} = \begin{bmatrix}\mathbf{0} & \mathbf{A}; & \mathbf{0} & \mathbf{0}\end{bmatrix}, \tag{11}$$

the input power P_{in} is given as $P_{\text{in}} = \frac{1}{2}\mathfrak{Re}\{\mathbf{w}^H\mathbf{P}_{\text{in}}\mathbf{w}\}$, so that the power transfer ratio P_{tr} can be written as

$$P_{\text{tr}} = \frac{P_{\text{out}}}{P_{\text{in}}} = \frac{\mathfrak{Re}\left\{\mathbf{w}^H\mathbf{P}_{\text{out}}\mathbf{w}\right\}}{\mathfrak{Re}\left\{\mathbf{w}^H\mathbf{P}_{\text{in}}\mathbf{w}\right\}} = \frac{\mathbf{w}^H[\mathbf{P}_{\text{out}}+\mathbf{P}_{\text{out}}^H]\mathbf{w}}{\mathbf{w}^H[\mathbf{P}_{\text{in}}+\mathbf{P}_{\text{in}}^H]\mathbf{w}}. \tag{12}$$

The objective is to determine $\mathbf{w}$ that maximizes (12) at a stationary point[1], i.e., $\boldsymbol{\nabla}_{\mathbf{w}^H}P_{\text{tr}}(\mathbf{w},\mathbf{w}^H) = 0$, which leads to the generalized eigenvalue equation [10, Sec. 10.2]

$$[\mathbf{P}_{\text{out}}+\mathbf{P}_{\text{out}}^H]\mathbf{w} = P_{\text{tr}}[\mathbf{P}_{\text{in}}+\mathbf{P}_{\text{in}}^H]\mathbf{w}. \tag{13}$$

Hence, maximizing (12) is equivalent to finding the largest positive eigenvalue P_{tr} in (13). Once the optimal $\mathbf{w} = \mathbf{w}_{\text{opt}}$ is found, the currents $\boldsymbol{J}$ and $\boldsymbol{M}$ can be computed through (3).

IV. Numerical Results

A. Basis Function Choice and Optimization Results

We employ a rectangular grid of pulse basis function currents and assume an x-polarized electric aperture field. The basis function currents are modeled as

$$\boldsymbol{f}_n(\boldsymbol{r}) = \hat{\boldsymbol{x}}\Pi(\boldsymbol{r}_n) \quad \text{and} \quad \boldsymbol{g}_n(\boldsymbol{r}) = \hat{\boldsymbol{y}}\Pi(\boldsymbol{r}_n) \tag{14}$$

where $\Pi(\boldsymbol{r}_n)$ is the support of the nth pulse basis function of size $(0.1\lambda)^2$ with centroid $\boldsymbol{r}_n$.

In the following, muscle tissue ($\epsilon_r = 57$, $\sigma = 1.2$ S/m) and/or fat ($\epsilon_r = 4.6$, $\sigma = 0.02$ S/m) are used as the lossy medium at 1 GHz [11].

As an example, the normalized amplitude and phase of the optimized electric currents for a pair of $2\lambda\times2\lambda$ apertures with 4λ spacing in muscle tissue are plotted in Fig. 2. The magnetic currents are not shown since the solution turns out to resemble a Huygen's source. More specifically, $\boldsymbol{M}(\boldsymbol{r}) \approx \eta^*\hat{\boldsymbol{n}}_1\times\boldsymbol{J}(\boldsymbol{r})$. As expected, the source current distribution has rotational symmetry around the axis of both apertures; henceforth, all current distributions will be plotted along the x-axis only.

B. Changes in Transmitter Aperture Size

A uniform field aperture provides the highest directivity in the far-field in a lossless medium (not considering super-directivity) and is therefore chosen as a suitable reference field distribution to compare the P_{tr} of the optimized aperture field relative with a uniform one of the same size. As is evident from Fig. 3(a), the difference in P_{tr} between the optimal and uniform aperture field is negligible when both of the apertures are small, and it is only beyond a certain size that the optimal aperture field demonstrates a (small) advantage over the uniform one.

[1]Although $\mathbf{P}_{\text{in}}+\mathbf{P}_{\text{in}}^H$ is generally an indefinite matrix, it was numerically verified that by employing Huygen's source basis functions (constrained to positive input power), the same optimal P_{tr} value is achieved.

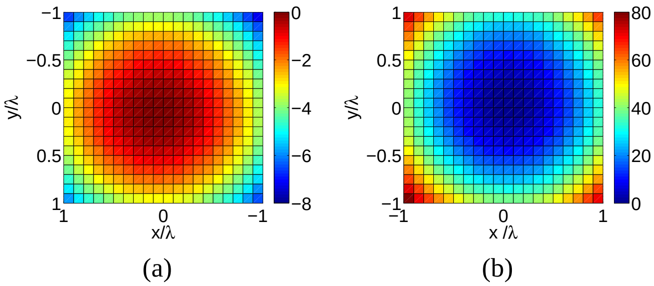

Fig. 2. (a) Amplitude in dB and, (b) phase in degrees, of the optimized electric current distribution on the transmitter aperture. The transmitter and receiver aperture sizes are $2\lambda \times 2\lambda$, located 4λ away from one another.

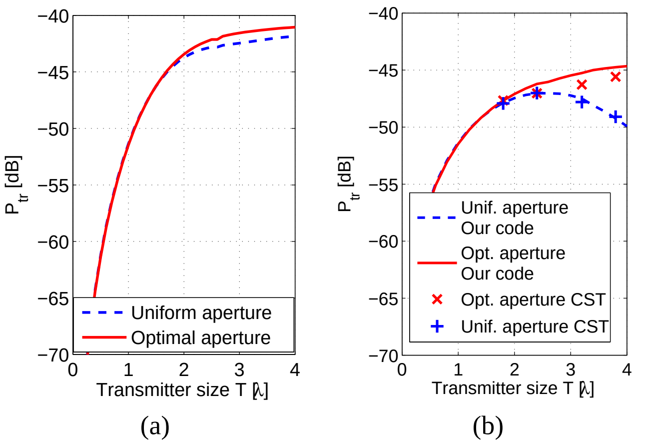

Fig. 3. Comparison of the power transfer ratio of the optimal and uniform apertures vs. the aperture size in muscle tissue (aperture separation distance is 4λ). (a) The transmitting and receiving apertures are of the same size. (b) The receiving aperture size is fixed at $1\lambda \times 1\lambda$.

However, in many practical cases, the receiver aperture must be of a limited size. Fig. 3(b) shows, for the uniform aperture field case and for a fixed receiver aperture size of $1\lambda \times 1\lambda$, that P_{tr} reaches its maximum for a certain transmitter aperture size, beyond which it declines. Indeed, as the supplied power is uniformly spread over a larger area, a smaller portion of that can only be collected at the receiver aperture due to the lossy medium, while for the optimal case the aperture field is nonuniformly spread to compensate for this reduction and instead will level out at a maximum P_{tr} value. The saturation size at which this happens depends on the size of the receiving aperture, distance d between the apertures, and the loss factor of the medium. The two apertures are also modelled in CST for comparison, the CST simulation results are shown in Fig. 3(b) and are in good agreement with the rest of the results.

The amplitude and phase plots for a number of optimal transmitting apertures ($R = 1\lambda$, $d = 4\lambda$, muscle tissue) are shown in Fig. 4. Note that x along the horizontal axis is normalized to its maximum for each transmitting aperture size, implying that the $[-1, 1]$ span along the horizontal axis are entire aperture lengths. An increase in aperture size is seen to lead to a higher amplitude taper towards the aperture edges, meaning that the majority of the power is concentrated around the center of the transmitter aperture, thereby keeping the distance to the receiver aperture, and thus the path attenuation, small. As for the phase, an increase in aperture size results in

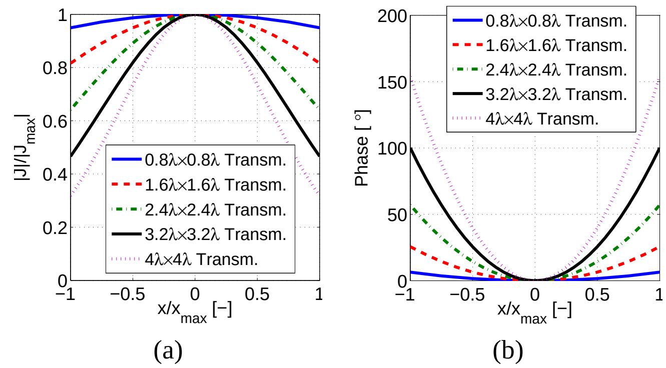

Fig. 4. (a) Normalized amplitude, and (b) phase in degrees, of the optimized electric current distribution on the transmitter aperture. The receiver size is $1\lambda \times 1\lambda$ located 4λ away from transmitter.

a larger phase lead taper towards the edges to constructively interfere the fields as the NF beam is focused. The optimal reference aperture field may be realized through a single (lens) antenna and/or an antenna array.

C. Transmitter and Receiver Aperture Distance Variations

To examine the effect of the spacing d between the two apertures, Fig. 5 shows a comparison of the P_{tr} values between the optimal and uniform apertures, but now for the larger distance $d = 8\lambda$ ($R = 1\lambda$, muscle tissue). Upon comparing this with Fig. 3(b), one can readily observe that: (i) P_{tr} reduces for increasing d, which is expected due to the field attenuation in the lossy medium; (ii) for transmitting apertures up to almost $3\lambda \times 3\lambda$, the optimal and uniform apertures provide almost the same P_{tr}, as compared to $2\lambda \times 2\lambda$ for $d = 4\lambda$ in Fig. 3(b), and; (iii) the size at which the uniform aperture provides its maximum P_{tr} increases with d.

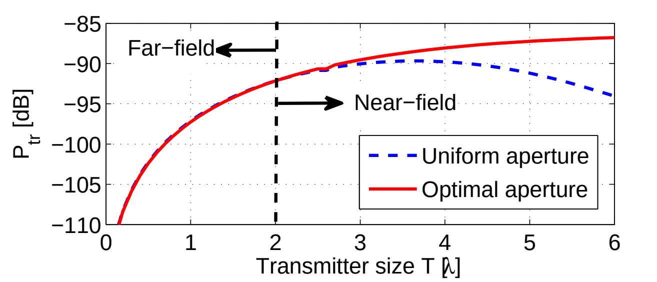

Fig. 5. Comparison of the power transfer ratio of the optimal and uniform aperture field cases vs. the aperture size for a receiver aperture of $1\lambda \times 1\lambda$. The aperture separation distance $d = 8\lambda$.

D. Changes in Receiver Aperture Size

Fig. 6 shows the P_{tr} value for the uniform and optimal aperture field cases ($d = 4\lambda$, muscle tissue) as a function of the transmitting aperture size for various different receiver aperture sizes. It is observed that the P_{tr} advantage of the optimal aperture field over the uniform one becomes higher for smaller receiver apertures, however, it should also be noted that a larger P_{tr} advantage occurs at a lower P_{tr} level. Since this affects the achievable signal-to-noise ratio and therefore the attainable receiving sensitivity, it should be taken into account

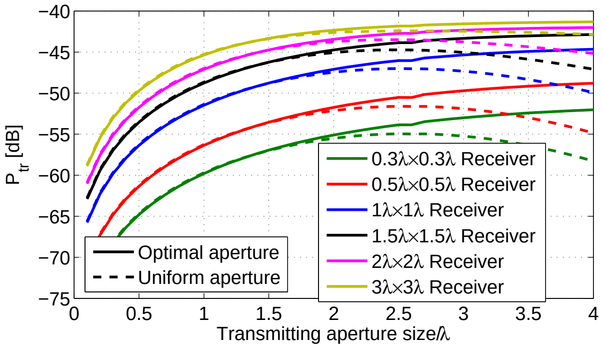

Fig. 6. Power transfer ratio from uniform and optimal apertures in muscle tissue, when the receiver aperture is located 4λ away from the transmitter for different sizes of receiver aperture vs. the size of transmitting aperture.

whilst selecting a proper size for the receiver antenna; a small receiver antenna simplifies the system design and the optimal aperture can provide a large P_{tr} advantage, but the received signal level should not be lower than the sensitivity of the electronics in order for the whole system to work.

E. Design Curves

Plots that show the optimal transmitting aperture size along with the achievable P_{tr} advantage relative to the uniform aperture field case are indispensable during NF system design phases. In the following, we consider the case where the receiver aperture size R and aperture separation distance d are constrained (i.e. fixed), while the best possible transmitting aperture is synthesized. For the purpose of developing design curves, P_{tr} for the optimal aperture as a function of the transmitter size T is computed, up to a point where P_{tr} increases less than 0.1dB per 0.2λ increase in T – we call this point T_{opt}. Accordingly, P_{tr} is computed for the uniform aperture field and its maximum is found. The P_{tr} advantage PA is then defined as the difference between the so-determined maximum values (*cf.* also Fig. 7). This, in turn, allows us to plot T_{opt} and PA as a function of d for various R.

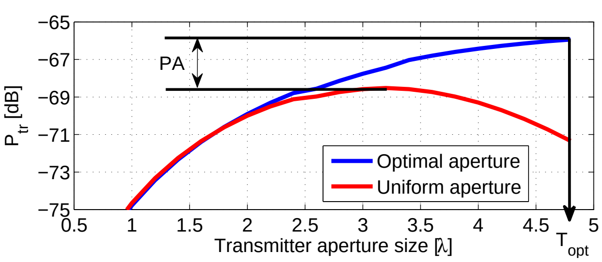

Fig. 7. Definition of different parameters in determining the design curves for specific values of R and d.

Fig. 8(a) and (b) show T_{opt} and PA as a function of d for various values of R both in muscle tissue and fat. As an example, assume that the objective is to design a transmitter antenna where, due to size constraints, d equals 5λ and the receiver size is $1\lambda \times 1\lambda$. With reference to Fig. 8(a), the size of the optimal aperture should then be selected as $T = 4.4\lambda$. If a larger transmitter aperture is used, the increase in P_{tr} will be very small. On the other hand, Fig. 8(b) shows that by

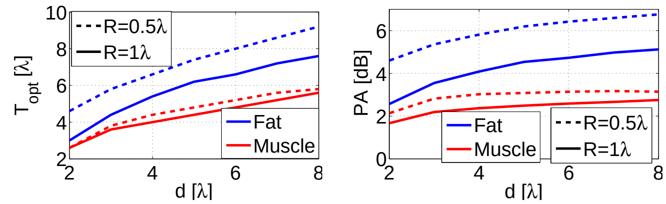

(a) (b)

Fig. 8. (a) The optimal size of the transmitter aperture, and (b) achievable P_{tr} advantage, both vs. distance between the antennas and for different receiver aperture sizes in fat and muscle tissue.

selecting the optimal aperture size and field distribution, a P_{tr} advantage of 2.5dB can be achieved. Fig. 8 shows that an increase in medium loss factor results in smaller T, however, this goes along with a decrease in PA as well.

V. Conclusions

An array-signal-processing-based numerical optimization method has been proposed that synthesizes the optimal transmitting aperture field distribution to maximize the power transmission between two aperture antennas in a lossy medium. The general modeling methodology and derived design curves are particularly useful for the design of wireless power transfer to implanted devices, detection of foreign objects in lossy materials, and near-field in-body communication systems; one can field-match the transmitting and receiving aperture antennas to the optimal reference fields, prior to fine-tuning the system. The effects of the transmitter and receiver aperture sizes, as well as the spacing between both apertures on the power coupling have been investigated and practical design curves for two representative media are presented.

References

[1] J. W. Sherman, "Properties of focused apertures in the fresnel region," *IEEE Trans. Antennas Propag.*, vol. 10, no. 31, pp. 399–408, Jul. 1962.

[2] R. C. Hansen, "Focal region characterisitics of focused array antennas," *IEEE Trans. Antennas Propag.*, vol. 33, no. 12, pp. 1328–1337, Dec. 1985.

[3] W. J. Graham, "Analysis and synthesis of axial field patterns of focused apertures," *IEEE Trans. Antennas Propag.*, vol. 31, no. 4, pp. 665–668, Jul. 1983.

[4] S. Karimkashi and A. A. Kishk, "Focused microstrip array antenna using a dolph-chebyshev near-field design," *IEEE Trans. Antennas Propag.*, vol. 57, no. 12, pp. 3813–3820, Dec. 2009.

[5] ——, "Focusing properties of fresnel zone plate lens antennas in the near-field region," *IEEE Trans. Antennas Propag.*, vol. 59, no. 5, pp. 1481–1487, May 2011.

[6] K. Sanghoek, J. S. Ho, and A. S. Y. Poon, "Wireless power transfer to miniature implants: Transmitter optimization," *IEEE Trans. Antennas Propag.*, vol. 60, no. 10, pp. 4838–4845, 2012.

[7] A. Razavi, J. Yang, and T. McKelvey, "Optimal aperture distribution of near-field antennas for maximum signal penetration," in *Proc. European Conference on Antennas and Propag. (EuCAP)*, Gothenburg, Sweden, Apr. 2006, pp. 279–283.

[8] G. V. Borgiotti, "Maximum power transfer between two planar apertures in the fresnel zone," *IEEE Trans. Antennas Propag.*, vol. 14, no. 2, pp. 158–163, Mar. 1966.

[9] M. V. Ivashina, M. N. M. Kehn, P.-S. Kildal, and R. Maaskant, "Decoupling efficiency of a wideband vivaldi focal plane array feeding a reflector antenna," *IEEE Trans. Antennas Propag.*, vol. 57, no. 2, pp. 373–382, Feb 2009.

[10] R. F. Harrington, *Field Computation by Moment Methods*. New York: The Macmillan Company, 1968.

[11] S. Gabriel, R. W. Lau, and C. Gabriel, "The dielectric properties of biological tissues: III. parametric models for the dielectric spectrum of tissues," *Physics in medicine and biology*, vol. 41, pp. 2271–2293, 1996.